Photoexcitation dynamics in polyfluorene-based thin films: Energy transfer and amplified spontaneous emission

Henning Marciniak,[1] Maik Teicher,[1] Ullrich Scherf,[2] Sara Trost,[3] Thomas Riedl,[3] Marcus Lehnhardt,[4] Torsten Rabe,[4] Wolfgang Kowalsky,[4] and Stefan Lochbrunner[1]

[1]*Institut für Physik, Universität Rostock, Universitätsplatz 3, 18055 Rostock, Germany*

[2]*Macromolecular Chemistry, Bergische Universität Wuppertal, Gaußstr. 20, 42119 Wuppertal, Germany*

[3]*Institute of Electronic Devices, Bergische Universität Wuppertal, Rainer-Gruenter Str. 21, 42119 Wuppertal, Germany*

[4]*Institut für Hochfrequenztechnik, Technische Universität Braunschweig, 38106 Braunschweig, Germany*

(Received 12 April 2012; revised manuscript received 7 June 2012; published 20 June 2012)

The dynamics of photoexcitations in thin films based on the polymer poly(9,9-dioctylfluorene) is investigated by a combination of stationary spectroscopy, femtosecond absorption and time-resolved fluorescence measurements. Excitation energy transfer to keto defects within the polyfluorene host matrix and to guest molecules in a dye doped host/guest system is observed and modeled by rate equations. Characteristic parameters for the exciton dynamics are extracted. At high excitation densities, amplified spontaneous emission from the edge of the films arises accompanied by strongly nonexponential signal decay in transient absorption. The underlying coupled excited-state and photon dynamics in the films are included in the model, which describes the measured data consistently for various excitation densities.

DOI: 10.1103/PhysRevB.85.214204 PACS number(s): 78.66.Qn, 78.47.da, 78.45.+h

I. INTRODUCTION

Polyfluorenes are a special class of conjugated polymers that have been subject to extensive scientific research for more than a decade;[1–3] their optical properties with emission wavelengths in the blue spectral region and high quantum yields make them interesting candidates for application in organic light emitting diodes (OLEDs) and solid state lasers.[4–7] Polyfluorenes can act as emitters themselves or serve as absorbing host materials for guest dyes that get excited via energy transfer and emit at longer wavelengths, thus enabling color tuning.[8,9] Poly(9,9-dioctylfluorene) (PFO) is a prototypical example. Aside from its potential for OLEDs,[2,5] light amplification has been observed in PFO waveguides as amplified spontaneous emission (ASE).[10,11] Thereby the emission wavelength has been shown to vary depending on the exact film morphology. Two different morphological phases were found to be important in PFO thin films:[3,12] a glassy phase and the β phase, which is characterized by a higher order of the polymer backbone accompanied by an increased π-conjugation length. Usually, both phases coexist in thin films, and the β phase acts as energy sink where excitations are trapped, thus causing a red shift of the emission wavelength.[10,13] It was shown that the formation of the β phase is efficiently suppressed by incorporating statistically intrachain 6,6′-(2,2′-octyloxy-1,1′-binaphtalene) binaphtyl spacer groups (BN) in the PFO matrix [BN-PFO, see Fig. 1(a)], while the optical properties of glassy PFO are preserved.[14] BN-PFO was employed in optically pumped thin film distributed feedback laser structures.[15,16] When acting as gain medium itself, the laser emission wavelength can be tuned between 435 and 465 nm. When employed as absorbing host material doped with the stilbene guest dye 1,4-bis(2-(4-(*N*,*N*-di(p-tolyl)amino)phenyl)vinylbenzene) [DPAVB, see Fig. 1(b)], the lasing wavelength is redshifted and tunable between 496 and 516 nm.[15] Furthermore, in the latter case, a lowering of the lasing threshold is achieved. However, for pump pulses with duration of more than a few nanoseconds, a decrease of laser emission is observed in the host/guest system, whereas pure BN-PFO shows stable emission. This can be explained by accumulation of triplet excitons during excitation, whose excited-state absorption overlaps with the emission wavelength of DPAVB and thus reduces the effective stimulated emission cross section.[16]

While these observations are made on a μs-timescale, a study of the photoexcitation dynamics of this system on the picosecond timescale, where energy transfer from the host to the guest can be assumed to take place, has not been carried out. In the present study, we use femtosecond transient absorption spectroscopy and time-resolved fluorescence measurements to investigate the photoinduced excitation dynamics in thin films made from BN-PFO containing 12% BN and of a host/guest system consisting of BN-PFO doped with 5 wt% DPAVB (BN-PFO/DPAVB). The energy transfer dynamics in the host/guest system BN-PFO/DPAVB, where Förster transfer to the guest dye DPAVB is intended to be the dominant process, is compared to the energy transfer to low-energy sites within the BN-PFO matrix, especially long-lived defect sites. It is known, that PFO, like other polyfluorenes, tends to build up keto defects in form of fluorenone units that act as efficient energy traps and lead to a broad green emission band peaking between 500 and 600 nm and an overall quenching of the quantum efficiency.[17,18] Hence a comparison of the underlying energy transfer dynamics to those defect sites with energy transfer to dopants is made. Furthermore, with regard to the potential for solid state lasing it is desirable to gain insight into the ASE characteristics. For this reason, the behavior of photoexcitations at high excitation densities, sufficient to cause ASE, is studied. Other PFO systems have been investigated by ultrafast spectroscopic techniques[19–21] and the results are compared to our findings. However, for BN-PFO, where the BN spacers serve to efficiently suppress the β phase, comparable studies are not available to the best of our knowledge.

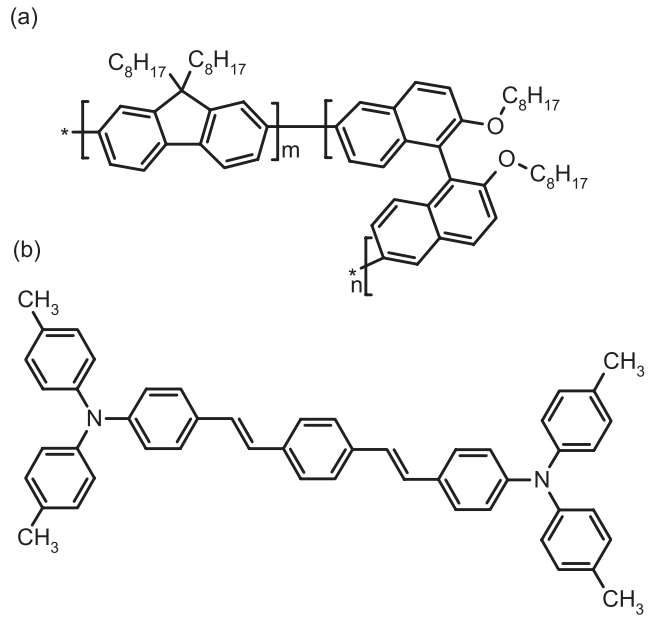

FIG. 1. (a) Structure of BN-PFO: poly(9,9-dioctylfluorene) (PFO) containing n/(m + n)% 6,6′-(2,2′-octyloxy-1,1′-binaphtalene) (BN). (b) Structure of 1,4-bis(2-(4-(*N*,*N*-di(p-tolyl)amino)phenyl)-vinylbenzene) (DPAVB).

II. EXPERIMENTAL

Thin films with a thickness of 175 nm of PFO containing 12% BN (BN-PFO) and of the same system doped with 5 wt% DPAVB (BN-PFO/DPAVB) were spin casted from toluene solution onto fused silica substrates of 1-mm thickness. The samples were kept under nitrogen atmosphere during storage. In the same way a thin film with a thickness of 140 nm of BN-PFO was prepared, containing a significant amount of keto defects as a result of a long storage time and repeated exposure to ambient atmosphere prior to the experiments (BN-PFO/defects). Furthermore, a thin film of pure DPAVB was thermally evaporated onto a fused silica substrate of 1-mm thickness under ultrahigh vacuum with a resulting film thickness of about 150 nm. Stationary absorption and fluorescence measurements of this film were made for comparison with signatures of DPAVB in the BN-PFO/DPAVB sample.

Stationary absorption and fluorescence spectra are measured with an UV-VIS spectrometer (Specord 50, Analytik Jena) and a spectrofluorometer (FluoroMax-4, Horiba Scientific), respectively. As excitation wavelength for the fluorescence measurements 388 nm is chosen in correspondence with the excitation wavelength of the time-resolved experiments.

Time-resolved fluorescence measurements are carried out after pulsed excitation at 388 nm with a streak camera system (Streakscope C10627, Hamamatsu) combined with a spectrograph (Acton Sp2150, Princeton Instruments), employing a grating with a groove density of 50 g/mm. The resulting time resolution is estimated from the full width at half maximum of the excitation pulse stray light signal to 110 ps for measurements up to a delay time of 10 ns. The excitation pulses are generated by frequency doubling the output of a 1 kHz regenerative Ti:sapphire amplifier system (CPA 2001; Clark MXR). The pulses have a duration of approximately 200 fs and are directed onto the sample under grazing incidence resulting in a spot size of approximately 0.2 cm^2. From there, the fluorescence is collected with two lenses with focal lengths of 50 mm collimating and focusing the emitted light onto the entrance slit of the spectrograph. The energy of the excitation pulses is attenuated to less than 10 nJ to keep the excitation density low.

The transient absorption measurements are performed with a setup similar to the one described in Ref. 22. The excitation pulses are generated in the same way as for the time resolved fluorescence measurements and focused to a spot size of several hundred micrometers in diameter which is considerably smaller than in the time-resolved fluorescence measurements. The spot size is determined by a beam camera (LaserCam-HR, Coherent). The transient absorption is probed by a white light continuum generated in an eccentrically moving 4-mm thick calcium fluoride substrate. After passing through the sample, where the probe beam is focused into the excited area, it is recollimated and dispersed with a prism. The transmitted probe energy is spectrally resolved measured with a multichannel detector based on a photo-diode array with 512 pixels. The polarizations of the pump and probe pulses are adjusted to 54.7° ("magic angle") with an achromatic $\lambda/2$-wave plate in the pump arm. In order to prevent degradation, the samples are kept under nitrogen atmosphere during the measurements and rotated to reduce the irradiation time of a single spot.

For data analysis of measurements with different excitation fluences, the density of excitons generated by the pump pulse has to be known. An average value for the exciton density in the probe volume is calculated according to the formula:

$$\langle n^* \rangle = \frac{N_{\text{pump}}}{\pi r_{\text{probe}}^2 d}[1 - 10^{-\text{OD}(\lambda_{\text{pump}})}]. \tag{1}$$

d is the thickness of the sample and $\text{OD}(\lambda_{\text{pump}})$ the optical density of the sample at the center wavelength $\lambda_{\text{pump}} = 388$ nm of the pump pulse. The intensity profiles of the laser beams are assumed to be Gaussian. The probe radius r_{probe} determines the area relevant for detection and is defined as the radius where the intensity of the probe beam is $1/e^2$ of the maximum intensity. The number of pump photons N_{pump} within this area is

$$N_{\text{pump}} = \frac{E_{\text{pump}}\lambda_{\text{pump}}}{hc} \frac{\int_0^{r_{\text{probe}}} re^{-\frac{2r^2}{r_{\text{pump}}^2}} dr}{\int_0^{\infty} re^{-\frac{2r^2}{r_{\text{pump}}^2}} dr}. \tag{2}$$

E_{pump} is the energy of the pump pulse and was in the range between 8 and 72 nJ during the transient absorption measurements. r_{pump} is the radius of the pump beam at the sample according to the $1/e^2$ criterion.

To detect amplified spontaneous emission (ASE) pulsed excitation at 388 nm with high excitation fluences of more than 100 $\mu J/cm^2$ is applied. The emission from the edge of the samples is collected with two lenses, collimating the light and focusing it onto the fiber tip of a fiber coupled spectrometer (USB4000, Ocean Optics).

III. RESULTS AND DISCUSSION

A. Energy transfer

The steady-state absorption and fluorescence characteristics of the samples are shown in Fig. 2. The absorption of BN-PFO is identical to absorption measurements of glassy PFO,[23–25] showing that the β phase is efficiently suppressed, while no additional absorption features due to BN are observed in the depicted spectral region. The fluorescence exhibits a dominating peak at 441 nm corresponding to the vibronic 0-1 transition. Moreover, two distinct shoulders can be observed, one on the blue side at 425 nm corresponding to the 0-0 transition and one on the red side due to the 0-2 transition, extending to 470 nm. The positions coincide with formerly published measurements.[23] The absorption and the fluorescence spectrum of BN-PFO/defects show essentially the same characteristics except of an additional broad emission band that appears in the fluorescence spectrum, centered in the green and extending from below 500-nm well into the red region above 600 nm. This band can be ascribed to emission from keto defects, i.e., fluorenone units in the polymer backbone that act as energy traps for photoexcitations.[17,18] The absorption spectrum of the BN-PFO/DPAVB sample is dominated by the absorption of the BN-PFO host matrix but shows an additional feature around 450 nm. This can be ascribed to the guest dye DPAVB and hints at a large overlap with the PFO emission thus potentially enabling efficient energy transfer.[26] This is confirmed by the fluorescence spectrum of BN-PFO/DPAVB whose double peak structure resembles the emission structure from pure DPAVB (not shown), though it is slightly blue shifted, probably due to a different environment of the guest molecules in the BN-PFO host matrix. Thus it can be concluded that efficient energy transfer from the host to the guest occurs. Direct excitation of the guest should be negligible compared to the dominant absorption of the host at the excitation wavelength (388 nm) and the low doping concentration.

In Fig. 3, streak camera measurements of the fluorescence of BN-PFO, BN-PFO/defects and BN-PFO/DPAVB are compared. The fluorescence of the pure BN-PFO sample is centered around 450 nm with a spectral distribution as expected from the steady-state measurements (see Fig. 2).

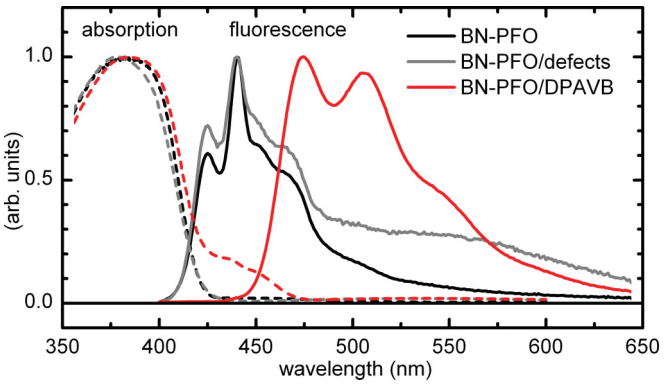

FIG. 2. (Color online) Absorption (dashed) and fluorescence (solid) spectra of the investigated thin film samples. All spectra are normalized to one at their maximum.

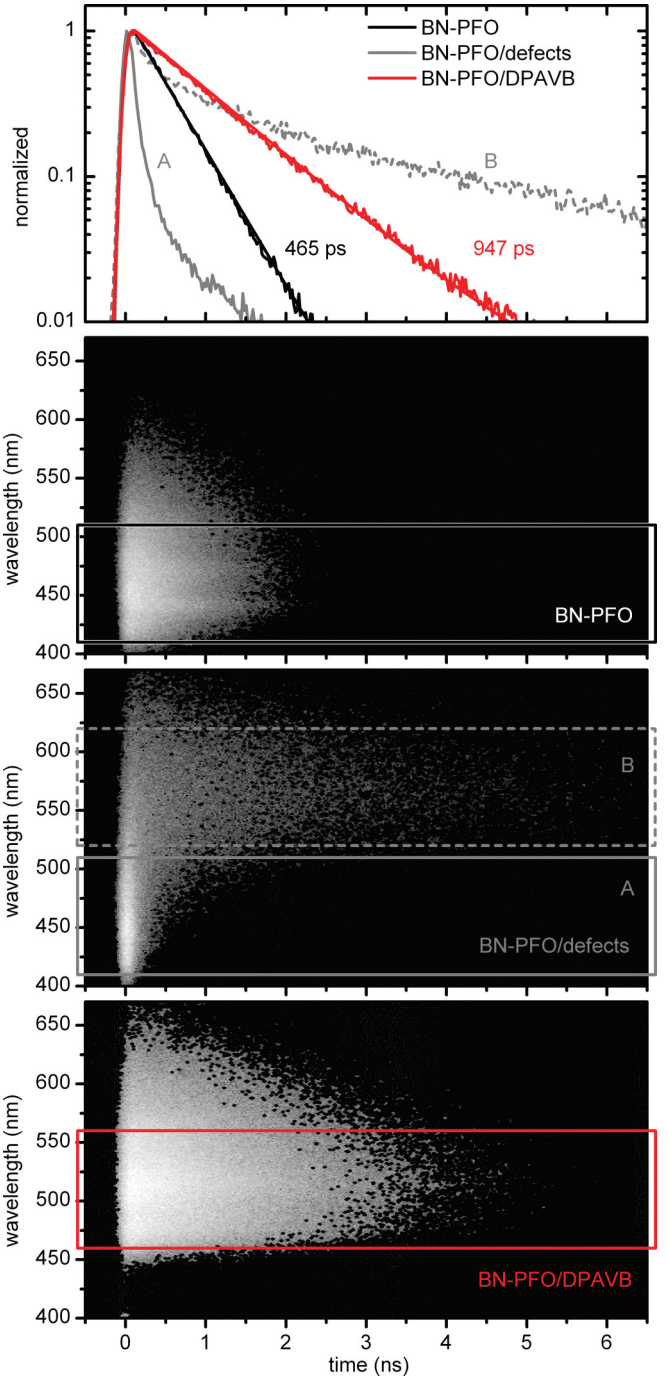

FIG. 3. (Color online) Time-resolved streak camera measurements of the fluorescence up to 6.5 ns after pulsed excitation at 388 nm. Upper panel: Time evolution of the integrated signal strength within the marked wavelength areas. The time traces are normalized to one at their maximum for better comparability. A logarithmic scale is chosen to illustrate the non / single exponential character of the decay dynamics.

It exhibits a monoexponential decay dynamics with a time constant of 465 ps in agreement with previously reported purely radiative decay times of PFO.[3,24,27] This implies that no significant quenching of the fluorescence takes place. The BN-PFO/defects sample shows in contrast a more complex fluorescence decay dynamics. Here the signal is dominated

by the PFO emission only at short times, nearly within the time resolution of the measurement, and does not exhibit a monoexponential behavior (trace A in Fig. 3). The center of the signal strength is subsequently shifted to longer wavelengths reflecting energy transfer to energetically lower lying molecular sites, i.e., defect sites. As a result, a broad redshifted fluorescence appears, with a decay time in the nanosecond regime (∼3.5 ns; trace B in Fig. 3), that is typical for excited keto defects.[3,28,29] This gives rise to the above mentioned green band in the stationary fluorescence spectrum (see Fig. 2). The streak camera measurement of the BN-PFO/DPAVB sample is clearly dominated by emission from the guest dye DPAVB as can be seen from comparison with the stationary measurements (see Fig. 2). The signal decays monoexponentially with a time constant of 947 ps that coincides well with the previously reported decay time of 900 ± 70 ps of DPAVB in a CBP (4,4′-di(*N*-carbozolyl)biphenyl) matrix.[30] The energy transfer process from host to guest seems to be much faster than the time resolution of the streak camera measurement, since signatures of PFO emission are completely absent. Hence a higher time resolution is needed to observe the transfer dynamics. This can be achieved by transient absorption measurements.

The upper panel of Fig. 4 depicts transient absorption spectra of the BN-PFO sample at several delay times after photoexcitation at 388 nm. The inset of the lower panel shows the time evolution of the transient signal at 445 nm and 650 nm. The transient spectra of BN-PFO are in agreement with formerly published measurements of PFO.[19–21] The region below 500 nm is dominated by stimulated emission (SE) from primarily generated singlet excitons with contributions from ground-state bleaching (GSB) close to 400 nm. Above 500 nm the spectra show excited-state absorption (ESA) that can also be attributed to singlet excitons since it has basically the same decay dynamics as the SE. The vibronic progression of the SE with the 0-0, 0-1, and 0-2 transitions around 420, 445, and 470 nm, respectively, is nicely resolved. At later delay times, a red shift of the spectral features compared to early times can be observed, e.g., the peak of the 0-1 transition shifts from 439 nm at 0.3 ps to 447 nm at 3 ps. This evolution can be explained with dispersive energy transport within the inhomogeneous density of states formed by the molecular sites of the polymeric film.[31] Due to the energetic disorder the photogenerated excitons have localized character and their migration can be modeled as an incoherent hopping process. Thereby an exciton preferentially migrates to a neighboring site with lower excitation energy, whereas thermal activation is needed to reach a site with higher excitation energy. Hence excitons generated on high-energy sites perform a "downhill migration" to lower energy sites.[32] This leads to an initially fast spectral shift that slows down until thermal equilibrium is reached. In contrast to the streak camera measurements the overall decay of the signal is significantly faster than the pure radiative decay of PFO and not monoexponential (see Fig. 4, inset). This acceleration can be explained by exciton-exciton annihilation that begins to appear at exciton densities of the order of 10^{18} cm^{-3} present here.[21,25] The complete dynamics can be modeled by the following differential equations:

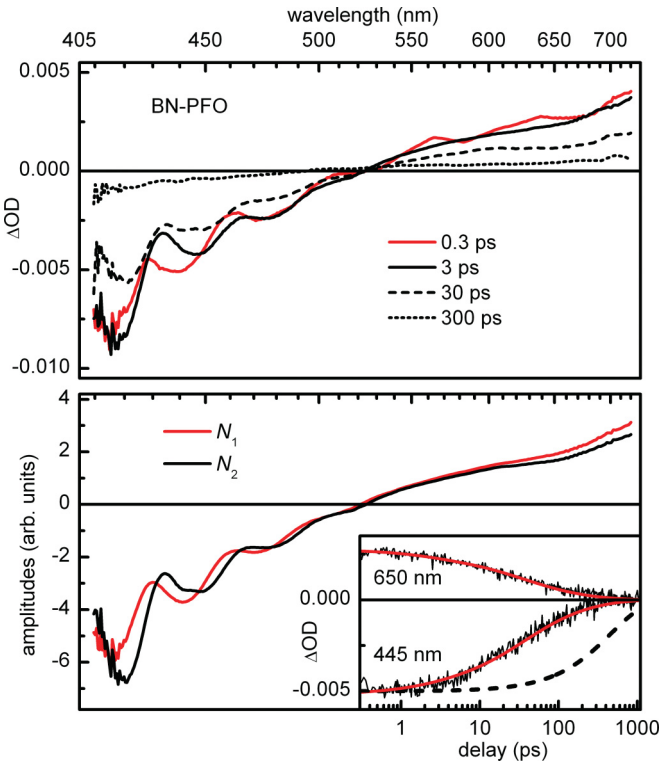

FIG. 4. (Color online) Upper panel: transient spectra of BN-PFO at different delay times after photoexcitation at 388 nm. A reciprocal wavelength scale is used to be linear in transition energy. Lower panel: associated amplitude spectra from the fit of the differential equations (3) and (4) (see text for further information). Inset: transient time traces (black) and fit curves (red) at 445 and 650 nm. The dashed line depicts a theoretical curve with an exponential decay time of 465 ps corresponding to the decay time of the streak camera measurement for comparison.

$$\frac{dN_1}{dt} = -(k_{\text{shift}} + k_{\text{rad}})\,N_1 - \gamma(t)N_1\,(N_1 + N_2)\,, \qquad (3)$$

$$\frac{dN_2}{dt} = k_{\text{shift}}N_1 - k_{\text{rad}}N_2 - \gamma(t)N_2\,(N_1 + N_2)\,. \qquad (4)$$

The spectral shift that can be seen in Fig. 4 is accounted for by introducing two species of singlet excitons with densities N_1 and N_2 that serve to parametrize the inhomogeneous distribution of excited states with N_2 being lower in energy than N_1. They are coupled by the rate k_{shift}. k_{rad} is the radiative decay rate and is adopted from the streak camera measurement with (465 ps)$^{-1}$. $\gamma(t)$ is the time-dependent rate for diffusion controlled annihilation given by[25,33,34]

$$\gamma(t) = \frac{1}{2}8D\pi R_a\left(1 + \frac{R_a}{\sqrt{2D\pi t}}\right) \qquad (5)$$

with the diffusion constant of the singlet excitons D. R_a denotes the critical distance between two excitons at which annihilation takes place and is set to 1 nm as an estimate for the average distance between molecular sites. The prefactor $\frac{1}{2}$ accounts for the assumption that only one exciton is destroyed in the course of an annihilation event.[33] It should be mentioned that more complex theoretical approaches exist to describe the excitation dynamics in conjugated polymer films, e.g., Monte-Carlo simulations based on a master equation

TABLE I. Summary of results from fitting our models [see Eqs. (3), (4), (6)–(8), and (10)–(12)] to the experimental data shown in Figs. 4–6. See text for further information.

$(k_{rad})^{-1}$	$(k_{shift})^{-1}$	D	$(k_{def})^{-1}$	ρ_{def}	$(k_{dye})^{-1}$	R_F	$(k'_{Fshift})^{-1}$
465 ps	2.25 ps	1.34 nm^2ps^{-1}	2980 ps	0.13×10^{-2} nm^{-3}	947 ps	4.30 nm	125 ps

approach and on quantum chemical calculations have been carried out.[31,35,36] However, to exploit the higher accuracy of those methods, a detailed knowledge of the structure of the investigated system is needed. The simpler rate equation approach applied here yet comprises the basic processes of the excitation dynamics and can be used to extract characteristic parameters. Equations (3) and (4) can be numerically fitted to the measured data yielding $k_{shift} = (2.25\ ps)^{-1}$ and $D = 1.34\ nm^2ps^{-1}$ (see also Table I). Similar values for D have been reported before for PFO films[21,25] thus indicating that the model is reliable while the BN-spacer groups do not affect the exciton dynamics significantly. Figure 4 (lower graph) also shows the associated amplitude spectra of the fit as well as the fit results at selected wavelengths (inset). The shape of the amplitude spectra corresponds to the shape of the transient absorption of the associated species. As expected the spectra of N_1 and N_2 exhibit essentially the same shape despite of a relative spectral shift.

The transient spectra of BN-PFO/defects (see Fig. 5. upper panel) strongly resemble the transient spectra of pure BN-PFO. The main difference is a further accelerated decay that might be seen best by comparing the transient spectra of BN-PFO and BN-PFO/defects at 30 ps after excitation. At longer delay times an additional ESA signature becomes evident with a weak maximum between 550 and 600 nm. In former publications, ESA signatures in this wavelength region have been assigned to a charged species, potentially polarons or polaron pairs.[19–21] Since the formation of polarons in polyfluorenes and phenylene-based polymers can result from charge transfer to defect sites,[1,17–19] this assignment is consistent with the observations in the steady state and the time-resolved fluorescence measurements of BN-PFO/defects. To model the exciton dynamics in BN-PFO/defects, the differential equations (3)–(4) are extended to include the defect states in the following way:

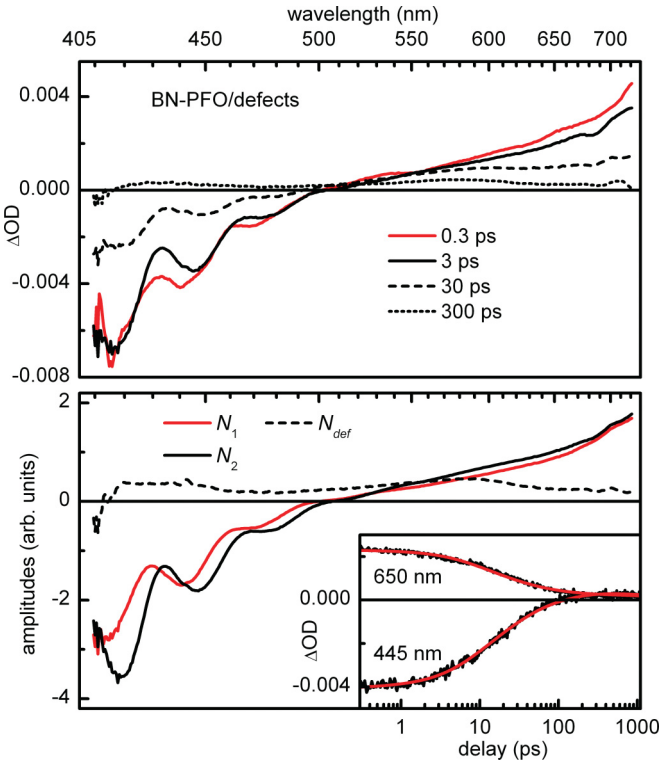

FIG. 5. (Color online) Upper panel: transient spectra of BN-PFO/defects at different delay times after photoexcitation at 388 nm. A reciprocal wavelength scale is used to be linear in transition energy. Lower panel: associated amplitude spectra from the fit of differential equations (6)–(8) (see text for further information). Inset: transient time traces (black) and fit curves (red) at 445 and 650 nm.

$$\frac{dN_1}{dt} = -(k_{shift} + k_{rad})N_1 - \gamma(t)N_1(N_1 + N_2) - \gamma'(t)N_1(\rho_{def} - N_{def}), \quad (6)$$

$$\frac{dN_2}{dt} = k_{shift}N_1 - k_{rad}N_2 - \gamma(t)N_2(N_1 + N_2) - \gamma'(t)N_2(\rho_{def} - N_{def}), \quad (7)$$

$$\frac{dN_{def}}{dt} = \gamma'(t)(N_1 + N_2)(\rho_{def} - N_{def}) - k_{def}N_{def}. \quad (8)$$

The rate $\gamma'(t)$ reads[33]

$$\gamma'(t) = 4D\pi R_a\left(1 + \frac{R_a}{\sqrt{D\pi t}}\right) \quad (9)$$

and accounts for the diffusion of mobile excitons with densities N_1 and N_2 to defect sites with density ρ_{def} that act as immobile traps. Thus a density of excited defect states N_{def} is created that decays with k_{def}. The difference between $\gamma(t)$ [see Eq. (5), exciton-exciton annihilation] and $\gamma'(t)$ [see Eq. (9), exciton trapping] is that in the former case the diffusion coefficient D is multiplied with 2 to account for the relative motion of excitons involved in an annihilation event. In the latter case, two different species, mobile excitons and immobile defect sites, are involved, both of which are destroyed in favor of a new species N_{def}. Hence no prefactor $\frac{1}{2}$ appears in formula (9). Numerically, fitting Eqs. (6)–(8) to the measured data of BN-PFO/defects results in $\rho_{def} = 0.13 \times 10^{-2}$ nm^{-3} and $k_{def} = (2980\ ps)^{-1}$ (see also Table I), which is in reasonable agreement with the results from the streak camera measurements. The numbers for k_{shift}, k_{rad}, and D are adopted from the numerical fit of the BN-PFO data. Based on the streak camera measurements, it is thereby assumed, that the spectral changes due to exciton diffusion to defect states can be temporarily separated from the initial spectral shift, since they are significantly slower. The amplitude spectra for N_1 and N_2 (see Fig. 5, lower panel) largely resemble the amplitude spectra

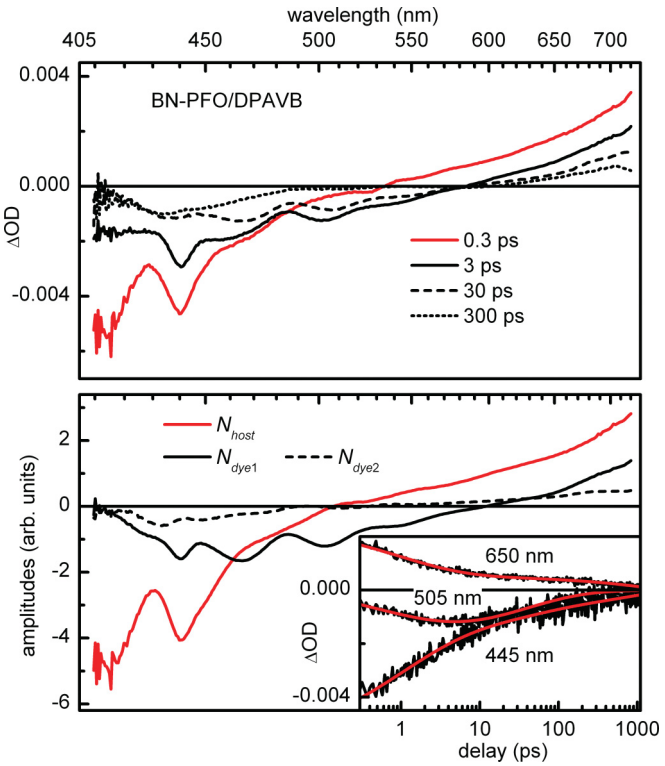

FIG. 6. (Color online) Upper panel: transient spectra of BN-PFO/DPAVB at different delay times after photoexcitation at 388 nm. A reciprocal wavelength scale is used to be linear in transition energy. Lower panel: associated amplitude spectra from the fit of differential equations (10)–(12) (see text for further information). Inset: transient time traces (black) and fit curves (red) at 445, 505, and 650 nm.

from Fig. 4 (BN-PFO), as expected, while the amplitude spectrum for N_{def} reflects the broad ESA of the transient spectrum at longer delay times.

The transient spectra of the host/guest system BN-PFO/DPAVB exhibit a distinctly different behavior (see Fig. 6, upper panel) from those of BN-PFO and BN-PFO/defects. Here, a very fast decay of the characteristic shape of the BN-PFO transient spectrum can be observed. More precisely the BN-PFO SE peak at around 440 nm is significantly steeper on the long wavelength side almost instantly after excitation. It disappears completely within the first few picoseconds mainly in favor of a new SE band around 500 nm, the typical emission region of DPAVB. The remaining negative signal around and below 450 nm can be explained as GSB from excited DPAVB molecules since it corresponds to the absorption signature of DPAVB identified in the steady state measurements (see Fig. 2). The SE signal around 500 nm is considerably smaller than that of PFO around 450 nm at earlier delay times and vanishes almost within 300 ps. This seems to contradict the time-resolved fluorescence measurements, which show a complete energy transfer to the guest dye and a resulting fluorescence lifetime of more than 900 ps (see Fig. 3). One reason for this might be a smaller transition dipole compared to the PFO that would cause a decrease of the signal and make the detection more difficult. Comparison of the radiative decay rates of PFO and DPAVB speaks in favor of this argument. For DPAVB the radiative decay rate was found to be $7.1 \times 10^8\ \mathrm{s}^{-1}$ in a CBP (4,4′-di(N-carbazolyl)biphenyl) host matrix[30] and thus about three times smaller than for PFO ($\sim 2.2 \times 10^9\ \mathrm{s}^{-1} \triangleq 450$ ps).[3,24,27] Another reason is certainly that ESA is superimposed in the transient measurements. For modeling the dynamics of the energy transfer it is assumed that the underlying process is Förster transfer. The spectral overlap of PFO fluorescence and DPAVB absorption suggests this. Because the energy transfer takes place very fast [with rate $k_F(t)$, see below] and dominates the dynamics during the short delay times, the spectral shift observed in the measurements of the BN-PFO and BN-PFO/defects samples can be neglected. Therefore the initially photogenerated singlet excitons of the host prior to the transfer to the dye are modeled as one species N_{host} in this case. However, it turns out that a two-species-model based on this assumption is not sufficient to describe the dynamics, especially at longer delay times where it should be determined by the guest dye DPAVB. Hence, in this case, a parametrization of the distribution of excited states of the excited dye molecules is applied. They are subdivided into two species N_{dye1} and N_{dye2}, representing slightly different transition energies with N_{dye2} being lower in energy than N_{dye1}. Because of a spectral overlap of DPAVB fluorescence and absorption (see Fig. 2) Förster energy transfer can occur between these species and may lead to a spectral shift that alters the transient dynamics of the BN-PFO/DPAVB sample as a whole. Inspection of the transient spectra actually shows a spectral shift of the SE signatures around 500 nm providing evidence for this notion. This leads to the differential equations:

$$\frac{dN_{\mathrm{host}}}{dt} = -k_{\mathrm{rad}} N_{\mathrm{host}} - \gamma(t) N_{\mathrm{host}}^2 - k_F(t) N_{\mathrm{host}}, \quad (10)$$

$$\frac{dN_{\mathrm{dye1}}}{dt} = k_F(t) N_{\mathrm{host}} - k_{\mathrm{dye}} N_{\mathrm{dye1}} - k_{F\mathrm{shift}}(t) N_{\mathrm{dye1}}, \quad (11)$$

$$\frac{dN_{\mathrm{dye2}}}{dt} = k_{F\mathrm{shift}}(t) N_{\mathrm{dye1}} - k_{\mathrm{dye}} N_{\mathrm{dye2}}. \quad (12)$$

The rates $k_{\mathrm{rad}} = (465\ \mathrm{ps})^{-1}$ and $k_{\mathrm{dye}} = (947\ \mathrm{ps})^{-1}$ are adopted from the time-resolved fluorescence measurements and $\gamma(t)$ from the numerical fit of the transient measurements on BN-PFO. The energy transfer rate $k_F(t)$ is meant to describe Förster transfer over a distribution of distances between donors and acceptors. It should be mentioned, that Förster theory of energy transfer is predicted to be inaccurate for donor-acceptor distances in the range of the chromophore size or shorter, due to the breakdown of the point dipole approximation used therein.[37] In particular, quantum-chemical calculations have shown that the energy transfer rate is overestimated for a cofacial arrangement of donor and acceptor, while it is underestimated in the case of a head-to-tail arrangement.[38,39] Thus in disordered systems like conjugated polymer films, cancellation of the errors might occur[39] and the application of more accurate theories is difficult due to the appearance of many different geometries and the limited knowledge about the specific structures. Assuming Förster energy transfer, $k_F(t)$ reads[33,40]

$$k_F(t) = \frac{2}{3} R_F^3 \sqrt{\frac{\pi^3 \frac{3}{2} \kappa^2 k_{\mathrm{rad}}}{t}} \rho_{\mathrm{dye}}. \quad (13)$$

Here, ρ_{dye} is the density of DPAVB molecules in the sample R_F is the Förster radius for the transfer processes and κ^2 is a factor accounting for the average relative orientation of the transition dipoles of host and dye molecules. For an amorphous film, κ^2 is 0.476.[41] Equation (13) was derived by Förster for the case of a single donor molecule surrounded by a statistic distribution of acceptor molecules in a medium.[40] An analogous situation in a polymeric host/guest system would exist, if energy transfer is only possible from host to guest, i.e., exciton diffusion in the host matrix is negligible. Occurrence of exciton diffusion, corresponding to energy transfer from donor to donor, has been shown to accelerate the overall energy transfer to acceptors.[42,43] Thus determining R_F on the basis of Eq. (13) is expected to overestimate the Förster radius.[44] Nevertheless, R_F may serve as a benchmark for comparison with other systems, since similar models have frequently been used.[23,33,45] With an assumed mass density of 1 g/cm^3 for the sample and the doping concentration of 5%wt. one can estimate ρ_{dye} to 4.5 $\times$ 10^{-2} nm^{-3}, corresponding to a typical distance of 2.8 nm between dye molecules. Based on this, the Förster radius resulting from a numerical fit of Eqs. (10)–(12) to the measured data is $R_F = 4.30$ nm. Interestingly, a Förster radius of 4.2 nm has been derived (employing a similar model) for energy transfer from PFO to tetraphenylporphyrin, which is a red light emitter.[23] Hence it might be concluded that by doping PFO films color tuning to different emission wavelengths can be realized with the same efficiency.

For the rate $k_{F\mathrm{shift}}(t)$ a similar $t^{-1/2}$ time dependence as for k_F(t) can be expected since it is also based on Förster transfer. However, it is not reasonable to extract a Förster radius because it takes place within the inhomogeneously broadened distribution of DPAVB states. By writing $k_{F\mathrm{shift}}(t)$ as

$$k_{F\mathrm{shift}}(t) = \sqrt{\frac{k'_{F\mathrm{shift}}}{t}} \tag{14}$$

the parameter $k'_{F\mathrm{shift}} = (125\ \mathrm{ps})^{-1}$ can be determined as a characteristic rate for the resulting spectral shift (see also Table I). The associated amplitude spectra of the species largely resemble the shape of the transient spectra at different delay times, which is reasonable for the assumption of efficient Förster transfer between the species.

B. Amplified spontaneous emission (ASE)

At higher excitation densities, a strongly nonexponential behavior with an almost steplike signal decrease at around 0.6 ps delay time is observed in the BN-PFO (see Fig. 7, upper panel) as well as in the BN-PFO/defects sample (not shown) while it is absent in BN-PFO/DPAVB. To analyze this behavior, a series of transient absorption measurements with different excitation fluences, resulting in different initial exciton densities, was carried out on BN-PFO. It is found that the dynamics can be explained by ASE. Because the thin films have a higher refractive index than the substrates on one side and the atmosphere on the other, they can act as waveguide for spontaneously emitted photons from photoexcited molecules. As those photons propagate through the film, they can stimulate the emission of other excited chromophores. In this way, an avalanche of photons is created in the direction of propagation until the excited states are

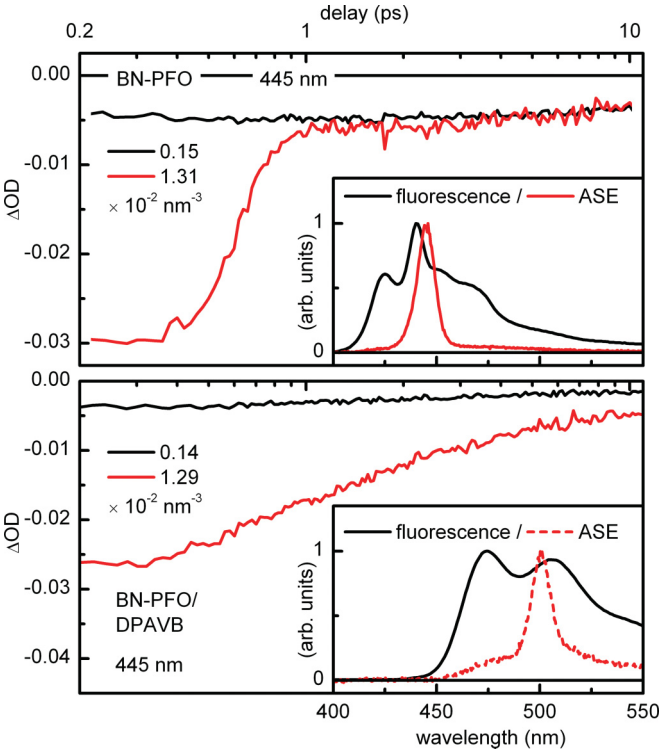

FIG. 7. (Color online) Transient absorption kinetics of BN-PFO (upper panel) and BN-PFO/DPAVB (lower panel) at 445 nm after photoexcitation at 388 nm with different excitation fluences (given are the resulting average initial exciton densities in units of 10^{-2} nm^{-3}). Inset: Fluorescence spectra after cw excitation (black) and ASE measurement after pulsed excitation (red) at 388 nm with high excitation fluence (see Sec. II for further information).

depopulated below a certain threshold.[46–48] This results in a burst of stimulated emission from the edge of the samples, which is accompanied by a fast depopulation of electronically excited states and a sharp signal decrease. The ASE burst is spectrally narrow and centered at the wavelength where the gain is highest. As can be seen in Fig. 7 (upper panel, inset), the BN-PFO sample shows spectral narrowing at around 445 nm, a typical ASE wavelength for glassy PFO.[10,11,48] The BN-PFO/DPAVB sample in contrast shows such a ASE burst at 500 nm (Fig. 7, lower panel, inset), where lasing from BN-PFO/DPAVB waveguide structures has also been observed.[15,16,49] This speaks in favor of the efficiency of energy transfer from PFO to DPAVB in the host/guest sample.

The dynamics due to the ASE in BN-PFO can be described by a system of coupled differential equations (on the basis of Ref. 46) that extends Eqs. (3)–(4) by including the interaction of molecular states with the photon density M:

$$\frac{dN_1}{dt} = -(k_{\mathrm{shift}} + k_{\mathrm{rad}})\,N_1 - \gamma(t)N_1\,(N_1 + N_2) - \frac{c}{n}\sigma\left(N_1 - \frac{N_1}{N_1 + N_2}G^*\right)M, \tag{15}$$

$$\frac{dN_2}{dt} = k_{\mathrm{shift}}N_1 - k_{\mathrm{rad}}N_2 - \gamma(t)N_2(N_1 + N_2) - \frac{c}{n}\sigma\left(N_2 - \frac{N_2}{N_1 + N_2}G^*\right)M, \tag{16}$$

$$\frac{dM}{dt} = f k_{\mathrm{rad}}(N_1 + N_2) + \frac{c}{n}\sigma(N_1 + N_2 - G^*)M - \alpha M, \tag{17}$$

$$\frac{dG^*}{dt} = \frac{c}{n}\sigma(N_1 + N_2 - G^*)M - k_{\mathrm{relax}}G^*. \tag{18}$$

The dynamics of M is initialized by a fraction f of spontaneously emitted photons that is waveguided within the thin film sample. f is estimated to 0.58 from

$$f = \frac{1}{2}\int_{\theta_{TR}} \sin\theta d\theta, \tag{19}$$

where θ_{TR} is the angle that spans the sector in which the condition for total reflection for spontaneously emitted photons within the sample is fulfilled (referring to a simple wave guide model, see, e.g., Ref. 50). M is then coupled to the exciton densities N_1 and N_2 by the effective stimulated emission cross section σ, c is the speed of light and n is the refractive index of PFO, which is taken to be 1.8.[11] The factor α denotes an overall loss rate of photons from the probed region. To fully account for all features of the signal decay over the probed wavelength range, an additional species G^* has to be introduced. It is populated via the ASE process and describes a vibrational excited ground state, analogous to the upper ground-state level in a four-level-laser system.[7] It relaxes with rate k_{relax} and thus leads to a delayed recovery of the original ground state. Without this process the delay of the sharp signal decrease at 410 nm, where the signal has a strong contribution from GSB, relative to 450 nm cannot be modeled (see Fig. 8). In addition, it has to be taken into account, that waveguided photons can be absorbed by G^* and thereby excitons N_1 an N_2 can be created with fractions that are estimated here with $N_1/(N_1 + N_2)$ and $N_2/(N_1 + N_2)$, respectively. With this model, the data of the transient measurements of BN-PFO with three different excitation fluences is numerically fitted. The average initial exciton densities are calculated from the excitation fluences, the optical density and the thickness of the sample (see Sec. II). The rates k_{shift}, k_{rad}, and $\gamma(t)$ are adopted from the numerical fit of Eqs. (3)–(4) to the measured data at low excitation fluence (see Fig. 4). The numbers for σ, α, and k_{relax} are obtained from fitting the data over a wavelength range from 410 to 720 nm for all three excitation fluences consistently.

The resulting numbers are given in Table II. They are reasonable and confirm the basic validity of the model. The effective cross section for stimulated emission σ is derived as 0.017 nm^2 and thereby within the range that would be expected for conjugated polymers,[4,46,48,49] comparable, e.g., to the value reported for ladder-type poly(p-phenylene)s of 0.015 nm^2.[46] However, this has to be seen as a weighted average over the wavelength range of stimulated emission. At the ASE wavelength of 445 nm, the cross section can be expected to be higher, though still of the same order of magnitude. The measure α as a loss rate of photons from the probed region can be expected to be of the order of $(c/n)/l$, where l denotes the characteristic path length a photon can travel before it is absorbed with $1 - 1/e$ probability. This leads to $l = 26.9\ \mu$m, which again has to be seen as a weighted average over the whole relevant wavelength region. Finally,

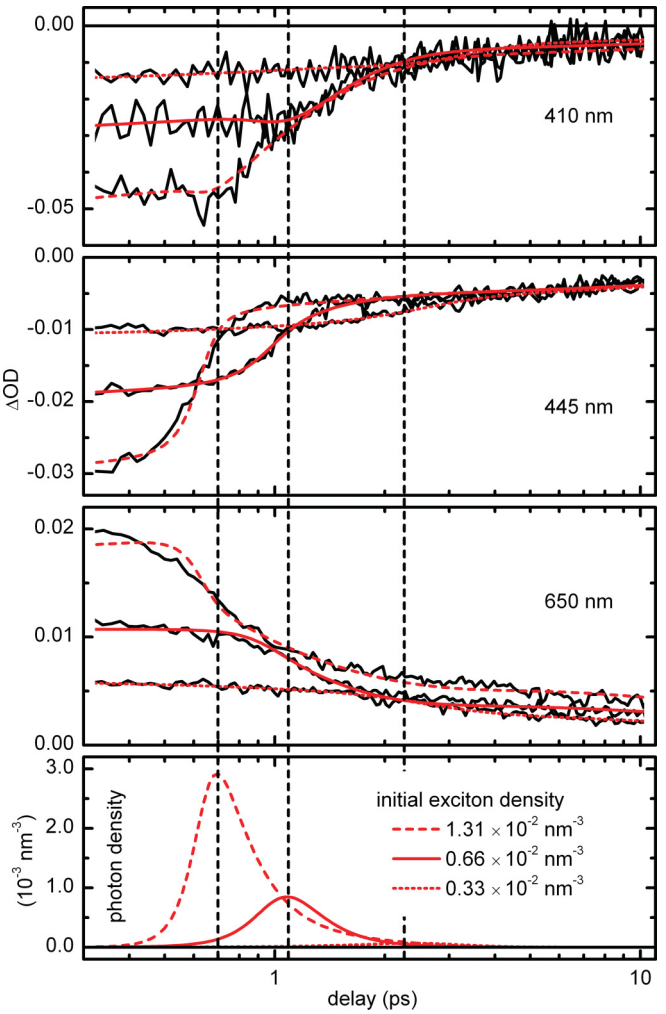

FIG. 8. (Color online) Fit results at selected wavelengths based on differential equations (15)–(18) after excitation of (pure) BN-PFO with different fluences (transient absorption data: black, fits: red). The lowest panel shows the time evolution of the photon density in the waveguide modes resulting from the fit and gives the corresponding initial exciton densities (see text for further information).

$k_{\mathrm{relax}} = (0.4\ \mathrm{ps})^{-1}$ is a typical vibrational relaxation time for organic molecules. Figure 8 shows time traces from the transient measurements and the corresponding fits at representative wavelengths. The evolution of the photon densities reflects nicely the nonlinearity of the process. ASE grows exponentially with time if a certain threshold for the excitation density, governed mainly by the loss factor α, is reached. The rate with which the photon density grows is determined by the exciton densities N_1 and N_2 [see Eq. (17)] and thus scales approximately with excitation fluence at early times. This is reflected in the experiments by the shift of the steplike

TABLE II. Results from fitting the model corresponding to Eqs. (15)–(15) to the experimental data shown in Fig. 8. See text for further information.

σ	α	$(k_{\mathrm{relax}})^{-1}$
0.017 nm^2	6.2 ps^{-1}	0.4 ps

signal decay with excitation fluence to shorter times which coincide with the peaks of the ASE (see Fig. 8). In principle, the model can account for the system BN-PFO/defects, too, though a smaller effective cross section for stimulated emission of 0.012 nm^2 results (not shown), which can be explained by the presence of keto defects, inducing additional ESA (see Fig. 5).

IV. SUMMARY AND CONCLUSIONS

In summary, we compared the photoexcitation dynamics in thin films of the polyfluorene derivate BN-PFO with and without the presence of defect states and of the host/guest system BN-PFO/DPAVB on time scales from the femtosecond up to the nanosecond regime by a combination of spectroscopic techniques. A consistent picture of the energy transfer processes within the system was obtained.

It is found that the presence of keto defects in undoped BN-PFO films leads to a fast quenching of emission. Time-resolved fluorescence measurements illustrate that the underlying process of energy transfer to a broad distribution of defect states takes place in less than 100 picoseconds. Transient absorption measurements reveal nonlinear decay dynamics at sufficiently high exciton densities. From a numerical fit of a model based on exciton-exciton annihilation, an exciton diffusion constant of 1.34 nm^2ps^{-1} can be extracted and be used to consistently model the energy transfer to keto defects as diffusion controlled. This value for the diffusion constant is considerably higher than in poly(3-hexylthiophene) (0.18 nm^2ps^{-1})[51] and polyparaphenylene (0.43 nm^2ps^{-1}).[52] Taking into account the fluorescence lifetime $\tau = 465$ ps (see Table I) a diffusion length $L_D = \sqrt{6D\tau}$ of 61 nm can be derived, which is about 5–10 times larger experimental values usually reported for conjugated polymers.[35] Note, however, that this is only the case for defect free films. It has been predicted theoretically that the diffusion length is significantly shortened by the existence of trap sites.[35]

In the dye doped host/guest system BN-PFO/DPAVB, the energy transfer from the PFO host matrix to the guest is shown to be very efficient. It is completed within the time resolution of the time-resolved fluorescence measurement. The higher time resolution of the transient absorption measurements reveals that it takes place in less than ten picoseconds and can be assumed to be due to direct Förster transfer. A characteristic Förster radius of 4.30 nm can be deduced.

At higher excitation densities, ASE at 445 nm can be observed from the edge of the BN-PFO sample accompanied by strongly non-exponential depopulation dynamics at early delay times. The dynamics can be modeled by including the interaction of exciton states with the density of waveguided photons within the sample, giving a value for the effective stimulated emission cross section of 0.017 nm^2. In BN-PFO/DPAVB, the ASE from the sample edge appears at around 500 nm where lasing from the guest was observed when a similar BN-PFO/DPAVB system was employed as active medium in a distributed feedback structure.[15,16] Also the characteristic fast nonexponential decay observed in BN-PFO is lacking here (at the applied excitation fluences), hence speaking in favor of very efficient energy transfer to DPAVB.

ACKNOWLEDGMENT

Financial support by the German Science Foundation via the collaborative research center SFB652 “Strong correlations and collective effects in radiation fields: Coulomb systems, clusters and particles” is gratefully acknowledged.

[1] U. Scherf and E. J. W. List, Adv. Mater. **14**, 477 (2002).
[2] P. Chen, G. Yang, T. Liu, T. Li, M. Wang, and W. Huang, Polym. Int. **55**, 473 (2006).
[3] A. Monkman, C. Rothe, S. King, and F. Dias, Adv. Polym. Int. **212**, 187 (2008).
[4] U. Lemmer, Polym. Adv. Technol. **9**, 476 (1998).
[5] M. T. Bernius, M. Inbasekaran, J. O’Brien, and W. Wu, Adv. Mater. **12**, 1737 (2000).
[6] M. D. McGehee and A. J. Heeger, Adv. Mater. **12**, 1655 (2000).
[7] I. D. W. Samuel and G. A. Turnbull, Chem. Rev. **107**, 1272 (2007).
[8] C. Ego, D. Marsitzky, S. Becker, J. Zhang, A. C. Grimsdale, K. Müllen, J. D. MacKenzie, C. Silva, and R. H. Friend, J. Am. Chem. Soc. **125**, 437 (2003).
[9] G. Trattnig, A. Pogantsch, G. Langer, W. Kern, and E. Zojer, Appl. Phys. Lett. **81**, 4269 (2002).
[10] G. Ryu, R. Xia, and D. D. C. Bradley, J. Phys.: Condens. Matter **19**, 056205 (2007).
[11] H. Azuma, T. Kobayashi, Y. Shim, N. Mamaedov, and H. Naito, Org. Electr. **8**, 184 (2007).
[12] A. J. Cadby, P. A. Lane, H. Mellor, S. J. Martin, M. Grell, C. Giebeler, D. D. C. Bradley, M. Wohlgenannt, C. An, and Z. V. Vardeny, Phys. Rev. B **62**, 15604 (2000).
[13] M. Ariu, M. Sims, M. D. Rahn, J. Hill, A. M. Fox, D. G. Lidzey, M. Oda, J. Cabanillas-Gonzalez, and D. D. C. Bradley, Phys. Rev. B **67**, 195333 (2003).
[14] T. Rabe, M. Hoping, D. Schneider, E. Becker, H.-H. Johannes, W. Kowalsky, T. Weimann, J. Wang, P. Hinze, B. S. Nehls, U. Scherf, T. Farrell, and T. Riedl, Adv. Funct. Mater. **15**, 1188 (2005).
[15] T. Riedl, T. Rabe, H.-H. Johannes, W. Kowalsky, J. Wang, T. Weimann, P. Hinze, B. Nehls, T. Farrell, and U. Scherf, Appl. Phys. Lett. **88**, 241116 (2006).
[16] M. Lehnhardt, T. Riedl, U. Scherf, T. Rabe, and W. Kowalsky, Org. Electr. **12**, 1346 (2011).
[17] C. Gadermaier, L. Romaner, T. Piok, E. J. W. List, B. Souharce, U. Scherf, G. Cerullo, and G. Lanzani, Phys. Rev. B **72**, 045208 (2005).
[18] S. Gamerith, C. Gadermaier, U. Scherf, and E. J. W. List, Phys. Status Solidi A **201**, 1132 (2004).
[19] B. Kraabel, V. I. Klimov, R. Kohlman, S. Xu, H.-L. Wang, and D. W. McBranch, Phys. Rev. B **61**, 8501 (2000).
[20] S. Xu, V. I. Klimov, B. Kraabel, H. Wang, and D. W. McBranch, Phys. Rev. B **64**, 193201 (2001).
[21] M. A. Stevens, C. Silva, D. M. Russell, and R. H. Friend, Phys. Rev. B **63**, 165213 (2001).

[22]U. Megerle, I. Pugliesi, C. Schriever, C. F. Sailer, and E. Riedle, Appl. Phys. B **96**, 215 (2009).
[23]G. Cerullo, S. Stagira, M. Zavelani-Rossi, S. De Silvestri, T. Virgili, D. G. Lidzey, and D. D. C. Bradley, Chem. Phys. Lett. **335**, 27 (2001).
[24]A. K. Bansal, A. Ruseckas, P. E. Shaw, and I. D. W. Samuel, J. Phys. Chem. C **114**, 17864 (2010).
[25]P. E. Shaw, A. Ruseckas, J. Peet, G. C. Bazan, and I. D. W. Samuel, Adv. Funct. Mater. **20**, 155 (2010).
[26]T. Förster, Ann. Phys. **437**, 55 (1948).
[27]R. Xia, G. Heliotis, Y. Hou, and D. D. C. Bradley, Org. Electr. **4**, 165 (2003).
[28]S. I. Hintschich, C. Rothe, S. Sinha, A. P. Monkman, P. Scandiucci de Freitas, and U. Scherf, J. Chem. Phys. **119**, 12017 (2003).
[29]Y.-S. Wu, J. Li, X.-C. Ai, L.-M. Fu, J.-P. Zhang, Y.-Q. Fu, J.-J. Zhou, L. Li, and Z.-S. Bo, J. Phys. Chem. A **111**, 11473 (2007).
[30]T. Aimono, Y. Kawamura, K. Goushi, H. Yamamoto, H. Sasabe, and C. Adachi, Appl. Phys. Lett. **86**, 071110 (2005).
[31]S. C. J. Meskers, J. Hübner, M. Oestreich, and H. Bässler, J. Phys. Chem. B **105**, 9139 (2001).
[32]F. Fennel and S. Lochbrunner, Phys. Rev. B **85**, 094203 (2012).
[33]E. Engel, K. Leo, and M. Hoffmann, Chem. Phys. **325**, 170 (2006).
[34]H. Marciniak, X.-Q. Li, F. Würthner, and S. Lochbrunner, J. Phys. Chem. A **115**, 648 (2011).
[35]S. Athanasopoulos, E. Hennebicq, D. Beljonne, and A. B- Walker, J. Phys. Chem. C **112**, 11532 (2008).
[36]S. Athanasopoulos, E. V. Emelianova, A. B. Walker, and D. Beljonne, Phys. Rev. B **80**, 195209 (2009).
[37]D. Beljonne, C. Curutchet, G. D. Scholes, and R. J. Silbey, J. Phys. Chem. B **113**, 6583 (2009).
[38]K. F. Wong, B. Bagchi, and P. J. Rossky, J. Phys. Chem. A **108**, 5752 (2004).
[39]H. Wiesenhofer, D. Beljonne, G. D. Scholes, E. Hennebicq, J.-L. Bredas, and E. Zojer, Adv. Funct. Mater. **15**, 155 (2005).
[40]T. Förster, Z. Naturforsch. **4a**, 321 (1949).
[41]J. Baumann and M. D. Fayer, J. Chem. Phys. **85**, 4087 (1986).
[42]R. F. Loring, H. C. Andersen, and M. D. Fayer, J. Chem. Phys. **76**, 2015 (1982).
[43]R. J. D. Miller, M. Pierre, and M. D. Fayer, J. Chem. Phys. **78**, 5138 (1983).
[44]B. P. Lyons, and A. P. Monkman, Phys. Rev. B **71**, 235201 (2005).
[45]A. Dogariu, R. Gupta, A. J. Heeger, and H. Wang, Synth. Met. **100**, 95 (1999).
[46]A. Haugeneder, M. Neges, C. Kallinger, W. Spirkl, U. Lemmer, J. Feldmann, M.-C. Amann, and U. Scherf, J. Appl. Phys. **85**, 1124 (1999).
[47]C. Kallinger, S. Riechel, O. Holderer, U. Lemmer, J. Feldmann, S. Berleb, A. G. Mückl, and W. Brütting, J. Appl. Phys. **91**, 6367 (2002).
[48]F. Laquai, A. K. Mishra, K. Müllen, and R. H. Friend, Adv. Funct. Mater. **18**, 3265 (2008).
[49]T. Rabe, S. Döring, N. Hildebrandt, T. Riedl, W. Kowalsky, and U. Scherf, Mater. Res. Soc. Symp. Proc. **1197**, D01 (2010).
[50]P. K. Tien, Appl. Opt. **10**, 2395 (1971).
[51]P. E. Shaw, A. Ruseckas, and I. D. W. Samuel, Adv. Mater. **20**, 3516 (2008).
[52]V. Gulbinas, I. Mineviciute, D. Hertel, R. Wellander, A. Yartsev, and V. Sundström, J. Chem. Phys. **127**, 144907 (2007).